RSC Advances

ROYAL SOCIETY OF CHEMISTRY

www.rsc.org/advances

Cite this: DOI: 10.1039/c0xx00000x

www.rsc.org/xxxxxx

Full paper

The quantitative detection of the uptake and intracellular fate of albumin nanoparticles†

Liqun Jiang,‡[ab] Xin Zhao,‡[c] Chunli Zheng,[a] Fang Li,[ad] James L. Maclean,[e] Fangcheng Chen,[a] Archana Swami,[f] Hai Qian,[a] Jiabi Zhu,[a] and Liang Ge*[a]

Received (in XXX, XXX) Xth XXXXXXXXX 20XX, Accepted Xth XXXXXXXXX 20XX
DOI: 10.1039/b000000x

Little has been investigated about the intracellular fate of organic nanoparticles (NPs), which is important for the safety and drug delivery efficiency of NPs. In this study, to understand the NP cellular uptake and degradation characteristics, a quantitative method based on fluorescence resonance energy transfer (FRET) was developed and validated to detect the uptake and intracellular degradation of albumin NPs in MCF-7 cells. The effects of the crosslinking density and particle size on the intracellular uptake and degradation kinetics of albumin NPs were then systematically detected. The results indicated that the albumin NPs with higher crosslinking degrees could be internalized more quickly. With increasing NP diameter, the uptake number of NPs decreased, but the uptake NP weight increased due to the compensation of the increased weight of a single particle. The intracellular degradation results showed the NPs with a low crosslinking degree or a small diameter disassociated more quickly in cells, and the half-lives for the albumin NPs disassociation were in the range of 35-79h. These findings will provide fundamental but direct information for the optimal design and biomedical applications of NPs based on their intracellular fates, and the FRET method developed in this study can provide a novel and robust tool to track and monitor the NP intracellular fate.

Introduction

Due to the rapid development of material science and nanotechnology, biodegradable nano-sized drug delivery systems (NDDSs, such as nanoparticles, micelles, liposomes, etc.) have been extensively investigated for disease diagnosis[1-3] and treatment[4-6]. Till now, large amounts of functional NDDSs[7-13] have been proposed in labs or became pharmaceutical products, e.g. Abraxane®, Doxil®, Depocyt®, etc. but even the generally regarded safe carriers, such as the poly-ε-caprolactone (PCL), poly(DL-lactic acid), poly(lactide-cocaprolactone), and poly(lactide-co-glycide) (PLGA) nanoparticles (NPs), showed toxicity at high concentrations *in vitro* [14, 15]. Therefore, it's very important to obtain detailed information and develop quantitative tools about the cellular uptake and the intracellular fate of the biodegradable nanocarriers[6].

Although the kinetics and mechanisms of cellular uptake of NDDSs have been well documented[6, 16, 17], to our best knowledge, very few reports focused on the intracellular fate of these nanocarriers[18-21]. The lack of information on the intracellular fate, especially the intracellular degradation, not only made it difficult to design desired NDDSs, but also introduced excessive risk and sometimes even ethical problems for their future production and clinical application[22, 23].

Currently, the investigations of the NDDSs' intracellular fate were limited due to the immature quantitative detection method. For example, the method established for determination of PLGA NPs degradation in mice by detecting the molecular weight was limited by its low detection sensitivity and sample extraction difficulty[21], especially for the hydrophilic materials, which could hardly be extracted from the biological matrices efficiently. Another example is the coupled plasma mass spectrometry method developed for quantum dots intracellular elimination detection. This method may be applied only in the certain nano systems, which could release some elements or fragments with known molecular weights [24]. Therefore, a quantitative method with high sensitivity and widely applicable range is critical and highly needed for determining the NDDSs' intracellular fate detection.

Cite this: DOI: 10.1039/c0xx00000x

www.rsc.org/xxxxxx

Full paper

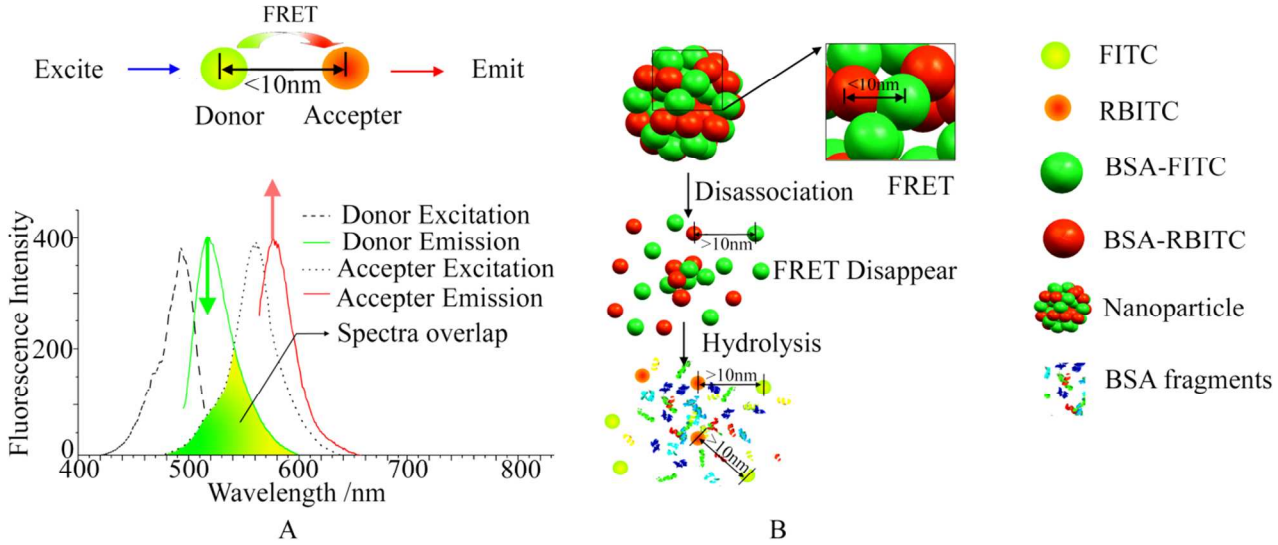

Fig.1 The requirements of FRET phenomenon (A) and the degradation process of FRET-based nanoparticles(B). The FRET phenomenon requires a high quantum yield of donor, the overlap of donor emission spectrum and accepter absorption spectrum and the donor-accepter distance <10nm. The degradation process of particles could be divided into the disassociation stage and the material hydrolysis stage. When the particle was disassociated, the donor-accepter distance was larger than 10nm leading to the disappearance of FRET phenomenon.

Fluorescence resonance energy transfer (FRET) involves the distance-dependent (<10nm) transfer of energy from a fluorescent donor in its excited state to another excitable accepter through a long-range nonradioactive dipole-dipole interaction[24] (Fig.1 A). As a powerful analytical technique for quantifying the distance between two fluorophores, it has been extensively and intensively utilized to interrogate changes in molecular conformation[25, 26], interactions of biomolecular machinery[27, 28], intracellular stability of polyplexes[29], etc.

In this report, the FRET theory was utilized and the NPs with FRET effect were designed to study the intracellular degradation of the NPs (Fig.1 B). In principle, in an intact NP, when the two dyes (the fluorescent donor and/or accepter labeled material), whose excitation and emission spectra overlap, are in sufficiently close proximity (<10nm), the excited-state energy of donor molecule is transferred to the neighboring accepter molecule, resulting in a quenching of donor and an enhancement of accepter. If the NP is disassociated, the donor-accepter distance is larger than 10nm, resulting the disappearance of FRET phenomenon. Therefore, a sensitive FRET-based method was developed and validated for the quantitative detection of NPs' intracellular degradation and fluorescein isothiocyanate (FITC) and rhodamin B isothiocyanate (RBITC) were selected as the fluorescent donor and accepter, respectively.

Albumin, a biodegradable, nontoxic and non-immunogenic protein, is an attractive material for NDDSs preparation[30], was selected as the building material for NP. Plenty of albumin nanocarriers[30-33] have developed to improve their pharmacokinetic and target behaviors, and the commercial albumin-bound paclitaxel (Abraxane®) had already shown good safety and efficiency in the clinical application[34, 35]. It has been reported that the both clathrin- and caveolae-mediated pathway could contribute to the intracellular endocytosis of albumin NPs[36], but the intracellular fate and the factors influencing the uptake and degradation of them were still unclear. In this report, as a model platform, a FITC or RBITC labeled bovine serum albumin (BSA) NP library was developed with different crosslinking degrees and diameters to investigate the uptake and intracellular degradation kinetics of NPs. Furthermore, the NPs' uptake pathway was also determined in this study.

Results and discussion

Albumin NPs preparation and characterization

To investigate the effects of physicochemical properties on the uptake and intracellular fate of BSA NPs, a BSA NP library was developed with a series of crosslinking degrees and diameters, but comparable zeta potentials (-20 ~ -30mV). These physicochemical properties are summarized in Table 1. The NPs with a series of crosslinking degrees from 41.9% to 91.1% (C40S70, C70S70 and C90S70) were obtained by reacting with different amounts of glutaraldehyde. The NPs (C40S70, C40S160 and C40S260) formulated with different albumin concentrations had comparable crosslinking degrees of about 42% but different diameters (71.8nm, 157.4nm and 261.9nm). The fluorescence emission spectra of these NPs were shown in Fig.2, and the highly quenching of donor and enhancement of accepter indicated the NPs possessed evident FRET effects, which guaranteed a significant fluorescence change even if only a tiny NPs disassociation occurred, thus providing a high sensitivity for the

NPs disassociation detection. The FRET indices of NPs with various diameters were about 23%; those of NPs with different crosslinking degrees were in the range of 23%～32% with larger indices being possessed by NPs of bigger crosslinking degrees, and this was perhaps because the chemical crosslink decreased the albumin molecular distances.

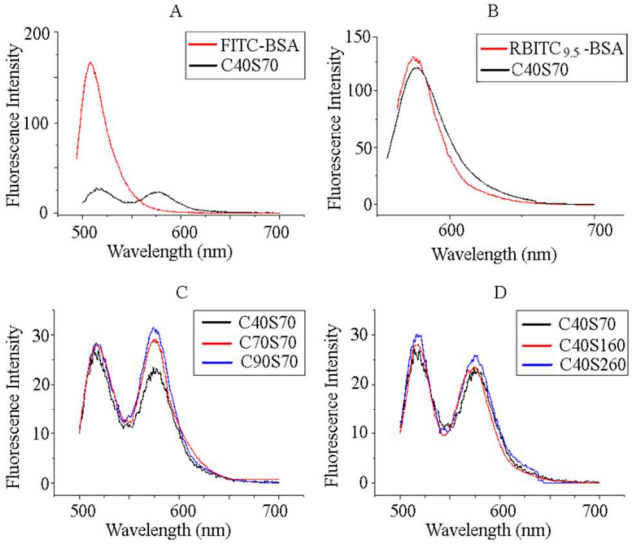

Fig.2 The fluorescence emission spectra of FITC-BSA (A), RBITC$_{9.5}$-BSA (B) and the albumin NPs with various crosslinking degrees (C) and diameters (D). A, C and D: excited at 488nm. B: excited at 548nm. The quenching of fluorescence donor and enhancement of accepter indicated the albumin NPs possessed evident FRET effects.

Table 1. Physicochemical properties of FRET-based BSA NPs

	Crosslinking Degree(%)	Diameter (nm)	Zeta Potential(mV)	FRET Index(%)
C40S70	41.9±1.5	71.8±0.1	-20.86±1.53	23.6±0.9
C70S70	66.2±2.1	72.0±0.1	-24.09±1.66	27.0±2.8
C90S70	91.1±0.8	71.7±1.4	-27.12±1.57	31.9±0.4
C40S160	42.3±1.0	157.4±2.3	-23.58±1.33	23.1±0.3
C40S260	41.8±1.1	261.9±1.2	-20.13±1.05	23.4±1.3

Validation of the NPs degradation detection method

To validate the method developed for the NPs degradation determination, the NPs with various crosslinking degrees and diameters were incubated in trypsin buffers, and the disassociation fractions and hydrolysis degrees [37] of NPs detected by the developed FRET-based method were compared with the results detected by the photometrical method[38] and the pH-stat method[39]. Different trypsin concentrations (6.6, 33, 66 and 100 μg/mL, pH8.0) were applied in this study, and the disassociation rates of C40S70 increased with the trypsin concentration as shown in Fig.3A1-A4. The first order disassociation rate constants were calculated as shown in Table 2. When the trypsin concentration was set at 66 and 100 μg/mL, comparing with those calculated by the photometrical method, significantly decreased disassociation rate constants were obtained by the FRET method; this is because when using the photometrical method, the

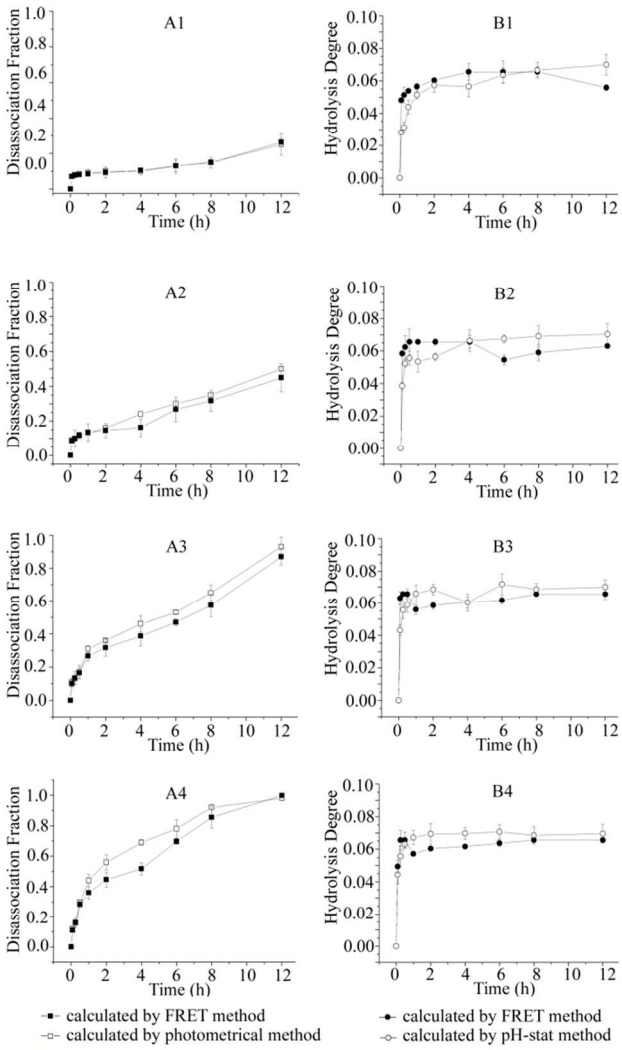

Fig.3 Validation of the FRET-based method by detecting the albumin NPs degradation in trypsin buffers. A: disassociation fractions determined by the FRET method and the photometrical method. B: values of DH determined by the FRET method and the pH-stat method. The trypsin concentrations were set at 6.6 (A1, B1), 33 (A2, B2), 66 (A3, B3) and 100μg/mL (A4, B4). (n=3)

intact NPs concentrations were underestimated for the rapidly decreased particle size brought in by the high trypsin concentrations. When the trypsin concentrations were set at 6.6 and 33 μg/mL, no significant difference of the disassociation rate constants were observed between the two methods. As shown in Fig.3B1-B4, similar results for the degree of hydrolysis (DH) were obtained by the FRET-based method and the pH-stat method: during the degradation process the values of protein DH reached the plateau rapidly, and the hydrolysis behaviors were independent on the trypsin concentration. These results indicate the FRET-based method works well for the NPs degradation detection, and this could also be concluded from the results of the other NPs (C70S70, C90S70, C40S160 and C40S260), which were shown in Fig.S1.

Table 2 Values of the disassociation rate constants of C40S70 in trypsin buffers detected by the photometrical method and the FRET-based method. (n=3)

Trypsin (μg/m L)	k^a (h^{-1})	k^b (h^{-1})
6.6	0.018±0.003	0.017±0.007
33	0.042±0.016	0.049±0.014
66	0.117±0.015**	0.179±0.015*
100	0.217±0.044*	0.302±0.033*

a: calculated from data detected by the FRET-based method
b: calculated from data detected by the photometrical method
*: p<0.05; **: p<0.01.

Cellular Uptake pathway

Besides macropinocytosis, which was the major pathway for microparticle internalization[40], there are three types of pinocytosis for NPs: clathrin-mediated pathway, caveolae-mediated pathway and clathrin- and caveolae-independent pathway[16, 41]. To detect the mechanisms involved in the uptake of albumin NPs in the MCF-7 cells, the uptake of albumin NPs in the presence of chemical inhibitors was measured as shown in Fig.3. A significant, but not complete, inhibition of uptake was observed in the presence of hypertonic medium, but no significant inhibition could be observed for all the NPs when using nystatin as the caveolae-mediated pathway inhibitor. The results showed that the uptake of the albumin NPs applied in this study was mainly via the clathrin-mediated endocytosis, and the uptake pathway was not influenced by the crosslinking degree and diameter of the albumin NPs.

Cellular uptake kinetics of albumin NPs

The membrane binding and intracellular uptake kinetics of the albumin NPs with different crosslinking degrees and diameters were detected in MCF-7 cells.

The effect of crosslinking degree on membrane binding and intracellular uptake of the albumin NPs are shown in Fig.5. The results showed that the membrane binding was almost saturated within 1h incubation, and NPs with higher crosslinking degree demonstrated a more efficient membrane binding. Compared with the intact NPs, the disassociated NPs in the membranes were negligible perhaps due to the lack of enzymes in the cell membranes. The intracellular uptake kinetics showed that the amount of intact albumin NPs increased within 6h, and a slight decrease was observed from 6 to 12h. Within the total incubation time of 12h, the amount of disassociated NPs inside the cells increased gradually. The total amounts of albumin NPs in the MCF-7 cells increased within 6h, at which time the uptake of C40S70, C70S70 and C90S70 plateaued, indicating saturation of uptake. The intracellular uptake kinetics showed the albumin NPs with higher crosslinking degrees (C90S70 and C70S70) were internalized more efficiently than those with a lower crosslinking degree (C40S70). A rapid hydrolysis of proteins disassociated from the NPs could be observed inside the cells as shown in Fig.5.

The influences of diameter on the albumin NP intracellular uptake kinetics were shown in Fig.6. For NPs with comparable crosslinking degrees but various diameters, a rapid saturation of the cell membrane-binding was observed, and with

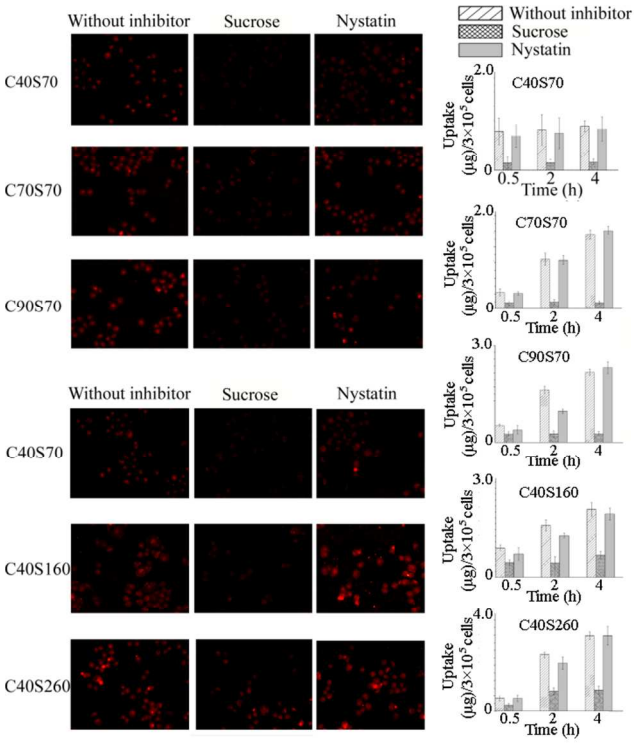

Fig.4 Effects of inhibitors on the intracellular uptake of albumin NPs. The inhibitors applied were sucrose (450mM) and nystatin (25μg/mL), which inhibited the clathrin-mediated and caveolae-mediated pathway, respectively. The inverted fluorescence microscope (Nikon Eclipse TI-5, Japan) was used for qualitative observation. The values of the intracellular uptake contents of NPs were obtained from the differences between the total cell-interacting and the membrane-binding data, which were detected at 37℃ and 4℃, respectively. (n=3)

increasing diameter, a significant increase of binding could be obtained. As shown in the figure, a gradual increase of the intact NPs and the total amount of the albumin NPs in MCF-7 cells could be observed during the first 6h, and the internalization increased with the increasing of particle size. The disassociated NPs inside the cells increased gradually within the period of 12h. When the number of particles instead of their weight was used as the unit of measurement, it was interesting to find that compared with C40S160 and C40S260 the NPs with a smaller diameter (71.8 nm, C40S70) had the most efficient uptake (Fig.7), concluding that the increase in diameter reduced the intracellular uptake particle number, but the weight of the intracellular particles was compensated by the increased weight of a single particle.

The cellular uptake kinetics of albumin NPs indicated the internalization of albumin NPs was controlled by the crosslinking degree and diameter of the NPs. As the nanoparticle-cell interface was the primary factor governing the interaction between particle and cell[42] and the NPs with various crosslinking degrees offered comparable diameter and zeta potential, the deviations in the uptake behaviors were thought to be due to the different surface chemistry caused by the various crosslinking degrees. As shown, the uptake of albumin NPs was mediated by the clathrin-mediated pathway, which involves the ligand-receptor interaction and receptor-mediated endocytosis. It was thought the crosslink reaction reduced the ligand density of the albumin NPs and

Cite this: DOI: 10.1039/c0xx00000x

www.rsc.org/xxxxxx

Full paper

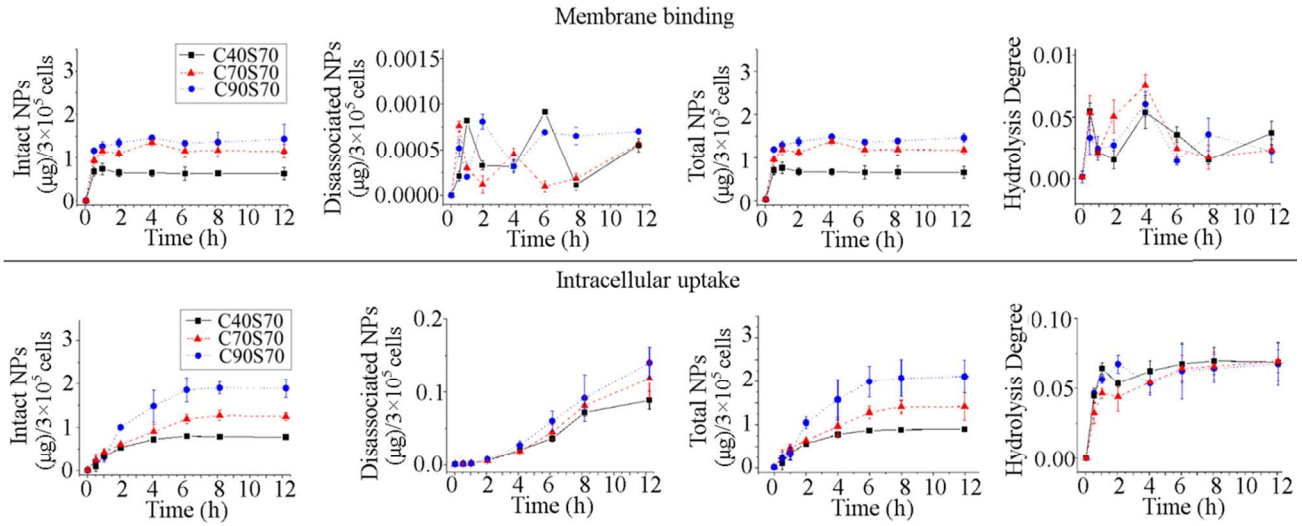

Fig.5 The membrane binding and cellular uptake of the albumin NPs with different crosslinking degrees (C40S70, C70S70 and C90S70). The MCF-7 cells were incubated with albumin NPs (37.5μg/mL) at 37℃ and 4℃ to detect the total cell-interacting and membrane-binding amounts of NPs. The intracellular uptake amounts were obtained from the differences between the total cell-interacting and the membrane-binding data. (n=3)

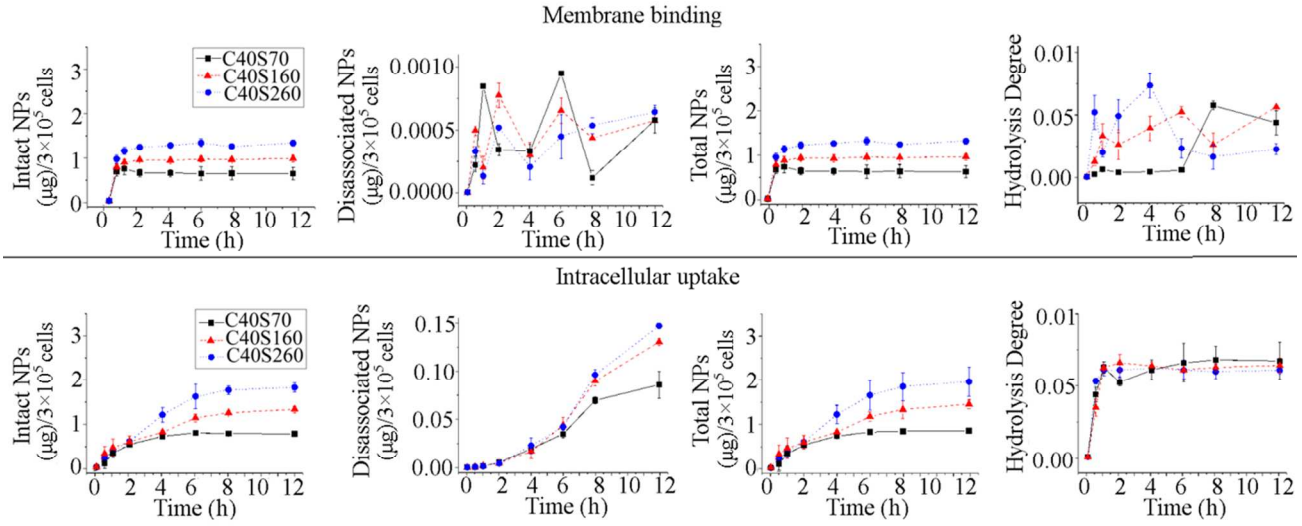

Fig.6 The membrane binding and cellular uptake of the albumin NPs with different diameters (C40S70, C40S160 and C40S260).The MCF-7 cells were incubated with albumin NPs (37.5 μg/mL) at 37℃ and 4℃ to detect the total cell-interacting and membrane-binding amounts of particles. The intracellular uptake amounts were obtained from the differences between the total cell-interacting and the membrane-binding data. (n=3)

consequently affected their cellular uptake. Yuan and Zhang[43] have theoretically elucidated the effects of ligand density and diameter on the kinetics of receptor-mediated endocytosis of NPs from thermodynamic aspect. It was revealed that because of the entropic penalty involved in ligand-receptor binding there existed an optimal condition (in terms of ligand density and diameter) at which the endocytic time is minimized. The time scale of full wrapping of NP was defined as l^2/D, where l was a characteristic length, and D was the diffusivity of the receptor. Here, the values of l^2 as the function of ligand density and diameter of the albumin NPs were calculated as shown in Fig.8. As shown, when the ligand densities were larger than the optimal one, the increasing of crosslinking density could decrease the ligand density and consequently decrease the wrapping time of the albumin NP. When the diameter of albumin NPs were all larger than the optimal one, the increasing diameter increased the wrapping time and consequently decreases the NP's cellular uptake.

The kinetics of disassociated NPs inside the MCF-7 cells was governed not only by the disassociation rate but also by the uptake of the NPs. Therefore, the degradation behaviors of these

NPs were determined in absence of uptake in the following studies to elucidate the effects of crosslinking degree and diameter of albumin NPs on their intracellular degradation behaviors.

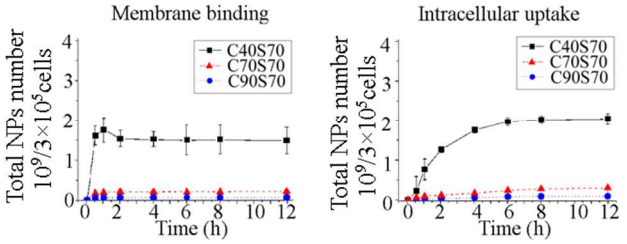

Fig.7 The membrane binding and cellular uptake of the albumin NPs with different diameters (C40S70, C40S160 and C40S260) using number as the unit of measurement. The number of NPs was calculated from the formula $6m/(\pi R^3\rho)$, where m was the weight of NPs, R was the diameter, and ρ was the density of NPs, which was determined as described by Ulbrich[44]

Intracellular degradation of albumin NPs

The intracellular degradation of albumin NPs was observed and detected based on the FRET phenomenon in absence of cellular uptake. As shown in Fig.9A, the signal of channel D could hardly be observed within the uptake of 2h. After 2h, the NP-containing medium was replaced by fresh NP-free medium to terminate the particle uptake, and after the subsequent incubation for 8h. Then a significant signal increasing from channel D (green fluorescence) could be observed for all the NPs (Fig.9B), indicating the disassociation of particles occurred within the subsequent 8h incubation.

The quantitative results of the NP's intracellular degradation were shown in Fig.10. For different amounts of NPs that were absorbed at the starting time of the degradation detection, the disassociated NPs were normalized by the initial NP content, and their disassociation fractions were obtained in the degradation detection. As shown in Fig.10A1 and B1, no significant change in the amount of total cell-associated NPs could be observed during the degradation detection, indicating the exocytosis of the albumin NPs was negligible within the time period of 8h. As shown in Fig.10A2, a decrease of the disassociation fraction were observed when the crosslinking degree increased, indicating that the albumin NPs with a lower crosslinking degree are disassociated more efficiently. With comparable crosslinking degrees, the NPs with a small diameter of 71.8 nm (C40S70) were disassociated more quickly than those with diameters of 157.4nm and 261.9nm (C40S160 and C40S260), indicating the intracellular disassociation rate of the particles was inversely related to the particle size (Fig.10B2). Quick and similar albumin hydrolysis behaviors of the NPs with different crosslinking degrees and diameters were observed in Fig.10A3 and B3.

The quantitative detection of NP degradation showed a gradual disassociation and quick hydrolysis of the particles in MCF-7 cells. The NPs with lower crosslinking degrees were disassociated more quickly in MCF-7 cells, indicating the extent of chemical crosslinking among the proteins was an important factor governing the NP's disassociation efficiency. The quick disassociation of the particles with smaller diameters may have resulted from the larger specific surface area and the consequently increased opportunities for the particle-enzyme interaction. Quick hydrolysis behaviors of the protein disassociated from NPs were observed in this study, indicating the disassociation was the rate-limiting step for the intracellular degradation of albumin NPs. The disassociation constants (k) of albumin NPs were obtained by fitting NPs' disassociation process using a first-order kinetic. The values of k and the half-lives of disassociation are shown in Table 3. When taking 5 times of half-lives as the washout period, after which more than 95% of NPs could be disassociated, the washout periods of albumin NPs applied in this study were in the range of 1-2.5 weeks. Although the data obtained in cell experiments could hardly represent *in vivo* results, it at least indicated the physicochemical properties of albumin NPs, such as their crosslinking degree and diameter, had an important impact on the clearance rate of NPs from the body and consequently on the safety of NPs.

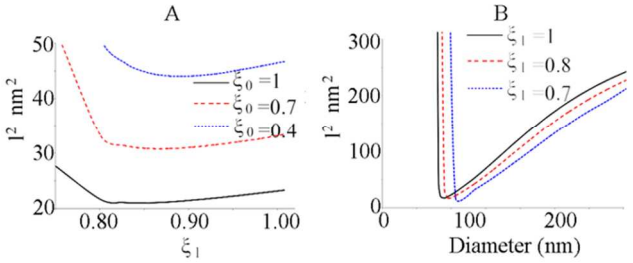

Fig. 8 The influences of ligand density (ξ_l) and diameter of the albumin NPs on the values of l^2, which was the characteristic length of the wrapping time scale of the NP ($t\sim l^2/D$) and was calculated as described by Yuan[43]. A: the diameter of albumin NPs were set at 72nm, and the average ligand density of the MCF-7 cell membrane was set at 0.4, 0.7 and 1.0. B: the ligand density was set at 0.7, 0.85 and 1.0, and the average ligand density of the MCF-7 cell membrane was set at 0.7

Table 3 Fitting of the intracellular disassociation processes of albumin NPs using a first-order kinetic.

	k (h^{-1})	R^2	$t_{0.5}$ (h)	washout time [a] (h)
C40S70	0.0192	0.9928	36.134	180.67
C70S70	0.0179	0.9839	38.619	193.095
C70S90	0.0160	0.9955	43.443	217.215
C40S160	0.0104	0.9854	66.359	331.795
C40S2601	0.0081	0.9940	85.939	429.695

a: the washout time was set as 5 half-lives, after which more than 95% of the albumin NPs could be disassociated.

Experimental

Materials

BSA (96%), fluorescein isothiocyanate (FITC, 90%), rhodamin B isothiocyanate (RBITC, labeling efficiency with bovine albumin >70%) and cysteine (97%) were purchased from Sigma-Aldrich. Trypsin was purchased from Hualan Chemical. Paraformaldehyde (99%) was purchased from Shanghai Lingfeng Chemical Reagent Co., Ltd. RPMI-1640 medium, fetal calf serum and antibiotics (penicillin 10,000units/mL, streptomycin 10,000μg/mL) were purchased from Hyclone Laboratories Inc.. All other reagents were analytical grade and were purchased from Nanjing Chemical Reagent Co., Ltd.

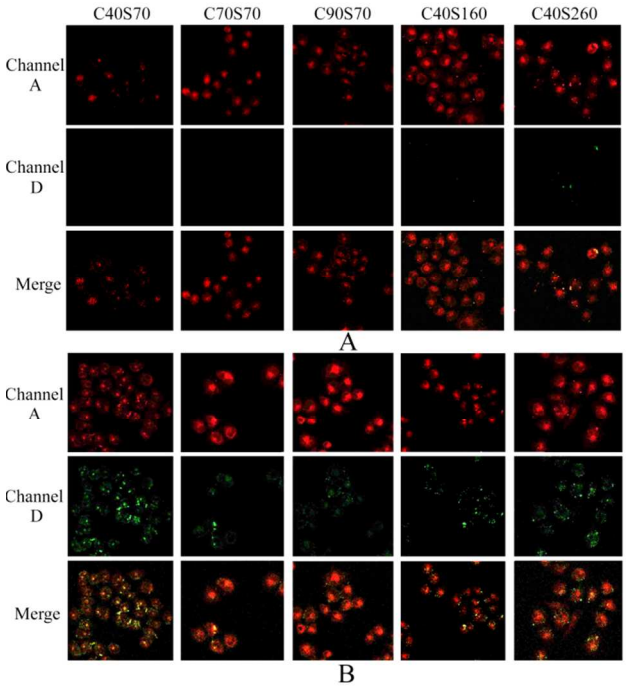

Fig.9 The uptake (A) and the degradation (B) of albumin NPs observed by the confocal laser scanning microscope (Leica TCS SP5, Leica, Germany). The uptake was observed after incubation of MCF-7 cells with albumin NPs for 2h, and the degradation was observed after the subsequent incubation of cells with the NPs-free medium for 8h.

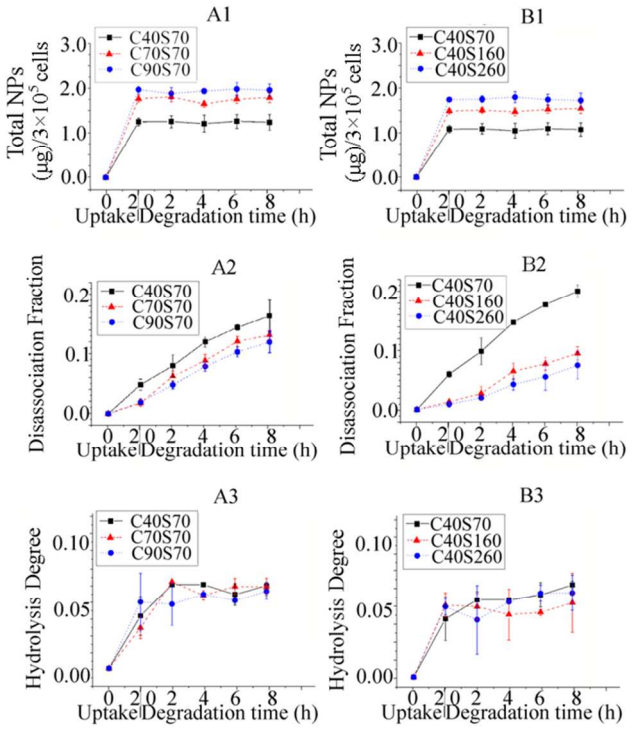

Fig.10 The degradation kinetics of albumin NPs with the series of crosslinking degrees (A) and diameters (B) within the uptake of 2h and the subsequent degradation of 8h in NPs-free medium. During the degradation of 8h, the total amounts of cell-interacting NPs (M+N) had no significant changes, indicating the exocytosis of the albumin NPs was negligible within 8h. The gradually increased disassociation fraction, which was calculated from N/(M+N), indicated the albumin NPs were degraded gradually in MCF-7 cells within the period of 8h. (n=3)

Albumin NPs preparation

FITC labeled BSA (FITC-BSA) and RBITC labeled BSA ($RBITC_{9.5}$-BSA) were synthesized by dissolving 100 mg BSA in 4mL of carbonate buffer and mixing with FITC (0.9 mg in 0.5 mL water) or RBITC (0.8mg in 0.8 mL DMSO). After incubation for 2 h and dialysis against deionized water for 24 h, the fluorophore labeled BSA would be obtained after freeze drying.

Then an albumin NP library with a series of crosslinking degrees (C40S70, C70S70 and C90S70) and particle sizes (C40S70, C40S160 and C40S260) were developed with FITC-BSA and $RBITC_{9.5}$-BSA using a disulfide bond reducing method established in our previous work[45]. Briefly, the mixture of $RBITC_{9.5}$-BSA and FITC-BSA with a weight ratio of 6:4 was dissolved in PBS buffer (pH8.0) at 85℃, and then a certain amount of cysteine was added to reach a final concentration of 5mg/mL. After dialysis against deionized water to remove the remnant cysteine, glutaraldehyde was added for the further crosslinking for 1h. The remnant glutaraldehyde was removed by dialysis and the albumin NPs were obtained by lyophilization. The formulation parameters of the albumin NP library are shown in Table 4.

Table 4 The formulation of albumin NPs prepared using the disulfide bond reducing method

	Protein Concentration[a] (mg/mL)	Glutaraldehyde: Protein (mg/mg)
C40S70	1	0.04
C70S70	1	0.1
C70S90	1	0.2
C40S160	2	0.04
C40S2601	4	0.04

a: The protein is the mixture of $RBITC_{9.5}$-BSA and FITC-BSA with a weight ratio of 6:4

NP characterization

Particle size and zeta potential measurement

The particle size and zeta potential of the NPs were determined using laser light scattering and a Zetaplus zeta potential analyzer (Brookhaven Instrument, USA), respectively.

Crosslinking degree determination

After adding the same volume of acetic acid-sodium acetate buffer (pH3.8) to the crosslinking reaction system, the NPs suspension was centrifuged at 8,000rpm for 30min at 4℃, and the supernatant was collected for glutaraldehyde detection. The crosslinking degrees of BSA NPs were determined using Eq. (1).

$$\text{Crosslinking Degree} = \frac{(m_{gluadd} - m_{glusupernatant}) \times M_{BSA} \times 2}{(m_{FITC-BSA} \times n_{FITC-BSA} + m_{RBITC_{9.5}-BSA} \times n_{RBITC_{9.5}-BSA}) \times M_{glu}} \quad \text{Eq(1)}$$

Where m_{guladd}, $m_{FITC\text{-}BSA}$ and $m_{RBITC9.5\text{-}BSA}$ were the amounts (g) of glutaraldehyde, FITC-BSA and $RBITC_{9.5}$-BSA added during the NPs preparation, respectively, and $m_{glusupernatant}$ was the amount (g) of glutaraldehyde in the supernatant after centrifugation at 8,000rpm for 30min at 4℃. M_{glu} and M_{BSA} are the molecular weight of glutaraldehyde and BSA, respectively.

The terms of $n_{FITC\text{-}BSA}$ and $n_{RBITC9.5\text{-}BSA}$ denoted the numbers of lysine in the molecule of FITC-BSA and $RBITC_{9.5}$-BSA, which provided the primary amines with the capability of reacting with glutaraldehyde.

FRET index determination

The efficiency of the donor-accepter energy transfer of the NPs was reflected using a FRET index, which was calculated by Eq.(2) [46].

$$\text{FRET Index} = \frac{F_b}{D_b} - \frac{F_d}{D_d} \quad \text{Eq(2)}$$

Where F_b and D_b are the fluorescence intensity of NPs in the channel F and D; F_d and D_d are the fluorescence intensity of FITC-BSA in the channel F and D. The detection of signals in different channels was described in details in Section "Sample fluorescence detection and data processing".

FRET-based method development

In the FRET-based method, the fluorescence intensity was detected in different channels (D, F and A), and the excitation and emission of these channels were listed in Table 5.

Table 5 The excitation and emission measurements of signals in channel D, F and A.

Channel	Excitation	Emission
D	Excitation of d (488 nm)	Emission of d (517 nm)
F	Excitation of d (488 nm)	Emission of a (576 nm)
A	Excitation of a (548 nm)	Emission of a (576 nm)

The samples of FITC-BSA (donor), $RBITC_{9.5}$-BSA (accepter) and NPs were termed *d*, *a* and *b*, respectively. The fluorescence intensity of samples was termed using the letters describing the sample and the channel. For example, D_d was the fluorescence of the donor in the channel D.

In this study, the degradation of NPs was divided into two steps as shown in Fig.1B: the disassociation of NPs and the hydrolysis of the protein disassociated from NPs. In the degradation process, the fluorescence intensity of samples was contributed by the intact NPs (M), the disassociated NPs (N) and the degree of hydrolysis [37] of protein disassociated. According to the contribution of M, N and DH, signals in channel D, F and A (F_D, F_F and F_A) can be described using the following equations.

$$F_D(M,N,DH) = F_{Db}(M) + F_{Dd}(N) \times f_{Dd} \quad \text{Eq.(3)}$$
$$F_F(M,N,DH) = F_{Fb}(M) + F_{Fd}(N) \times f_{Fd} \quad \text{Eq.(4)}$$
$$F_A(M,N,DH) = F_{Ab}(M) + F_{Aa}(N) \times f_{Aa} \quad \text{Eq.(5)}$$

Where F_{Db}, F_{Fb} and F_{Ab} were the fluorescence contribution of the intact NPs in channel D, F and A, and their standard curves were described by Eq.(6)-Eq.(8) using α and β as the slopes and intercepts of the standard curves. F_{Dd}, F_{Fd} and F_{Aa} were the fluorescence intensities of the disassociated NPs in channel D, F and A and their standard curves are described by Eq.(9)-Eq.(11), where n was the percentage of FITC-BSA in the NPs.

$$F_{Db}(M) = \alpha_{Db}C_M + \beta_{Db} \quad \text{Eq.(6)}$$
$$F_{Fb}(M) = \alpha_{Fb}C_M + \beta_{Fb} \quad \text{Eq.(7)}$$
$$F_{Ab}(M) = \alpha_{Ab}C_M + \beta_{Ab} \quad \text{Eq.(8)}$$
$$F_{Dd}(N) = \alpha_{Dd} \times n \times C_N + \beta_{Dd} \quad \text{Eq.(9)}$$
$$F_{Fd}(N) = \alpha_{Fd} \times n \times C_N + \beta_{Fd} \quad \text{Eq.(10)}$$
$$F_{Aa}(N) = \alpha_{Aa} \times (1-n) \times C_N + \beta_{Aa} \quad \text{Eq.(11)}$$

Where C_M and C_N are the concentrations of the intact NPs and the disassociated NPs. The slopes and intercepts in Eq.(6)-Eq.(11) could be obtained by plotting the fluorescence intensities in the corresponding channel against the concentrations of the samples.

Because of the self-quenching of FITC-BSA[47, 48] and $RBITC_{9.5}$-BSA as shown in Fig.S2, an increase of fluorescence can be attributed to the protein hydrolysis, and therefore the fluorescence intensities of the disassociated NPs (F_{Dd}, F_{Fd} and F_{Aa}) in Eq.(3)-Eq.(5) were corrected by the DH terms (f_{Dd}, f_{Fd} and f_{Aa}).The DH terms could be determined by plotting the fluorescence intensities against the DH of FITC-BSA and $RBITC_{9.5}$-BSA. Samples with different values of DH were prepared by digesting FITC-BSA and $RBITC_{9.5}$-BSA (2.5 mg/mL) in trypsin buffers at various concentrations. The DH of samples were detected using a pH-stat method[39]. The relationships between fluorescence increasing and DH of proteins were shown in Fig.S3, and it was found the DH terms of f_{Dd}, and f_{Fd} could be described using the linear equations (Eq.(12)-Eq.(13)). As shown in Fig.S3, a burst fluorescence increase was induced by the initial hydrolysis of $RBITC_{9.5}$-BSA (DH of 0.49%), and after the burst increase, the fluorescence intensity reached a plateau. To keep consistent with the formats of Eq.(12)-Eq.(13), a linear equation (Eq.(14)) was still used to express f_{Aa}, but the slope (α_{Aa}^{DH}) was set at 0 in the calculation.

$$f_{Dd} = \alpha_{Dd}^{DH} \times DH + \beta_{Dd}^{DH} \quad \text{Eq.(12)}$$
$$f_{Fd} = \alpha_{Fd}^{DH} \times DH + \beta_{Fd}^{DH} \quad \text{Eq.(13)}$$
$$f_{Aa} = \alpha_{Aa}^{DH} \times DH + \beta_{Aa}^{DH} \quad \text{Eq.(14)}$$

After substituting F_{Db}, F_{Fb}, F_{Ab}, F_{Dd}, F_{Fd}, F_{Aa}, f_{Dd}, f_{Fd} and f_{Aa} into Eq.(3)-Eq.(5), the unknown variables of M, N and DH could be obtained by solving the equation group using a sequential scanning method. A software program written in Visual Basic 6.0 was applied for the calculation.

Sample fluorescence detection and data processing

For the fluorescence detection, the fluorescence intensity of each sample in channel D, F and A were detected according to the excitation and emission method (Table 5) using the fluorescence spectrometer (RF 5301PC, SHIMADZU, Japan). The slit width of excitation and emission was set at 10 nm in this study. After substituting the fluorescence intensities into Eq.(3)-Eq.(5), the intact NPs content (M), the disassociated NPs content (N) and the hydrolysis degrees of proteins could be obtained by solving the equation group using the program provided in the Supporting Information.

Method validation

To validate the method developed in this study, the degradation of albumin NPs in trypsin buffer was measured, and the disassociation fractions and values of DH calculated using the FRET-based method were compared with the results obtained by the photometrical method and pH-stat method.

FRET-based method: NPs were suspended in the trypsin solution to a concentration of 500μg/mL at 37 ℃ under shaking, and the pH was adjusted to 8.0. After various time intervals (0.25, 0.5, 1, 2, 4, 6, 8 and 12h), 300μL of the sample was withdrawn and diluted with PBS buffer (pH8.0) to a volume of 3.0mL for the fluorescence analysis. The disassociation fractions and DH of the NPs were obtained by solving Eq.(3)-Eq.(5).

Photometrical method[38]: The disassociation fractions calculated from the FRET-based method were compared with the results detected by the photometrical method. After suspending

NPs in the trypsin solution, at the same time points mentioned above, 3mL of the sample was withdrawn for photometrical detection at 565nm. The NPs concentration was calculated using the calibration curve, and the disassociation fraction (DF) of the sample was calculated by Eq.(15). The calibration curve was obtained by plotting the turbidity of the NPs at 565nm against the NP's concentration.

$$\mathrm{DF} = 1 - \frac{\text{NPs Concentration}}{\text{Initial NPs Concentration}} \qquad \text{Eq.(15)}$$

pH-stat method[39]: The values of DH calculated from the FRET-based method were compared with those detected by the pH-stat method. At the same time points mentioned above, 10 mL of the sample was withdrawn, and the pH of the sample was adjusted to 8.0 using NaOH solution (1 M). The DH of the sample was calculated using Eq.(16).

$$\mathrm{DH} = \frac{C_{NaOH} \times V_{NaOH}}{\alpha \times h \times C_N \times V} \qquad \text{Eq.(16)}$$

Where C_{NaOH} and V_{NaOH} are the concentration and the volume of NaOH solution consumed for pH adjustment; C_N is the disassociated NPs concentration calculated by the photometrical method; V is the volume of the sample detected; α is the reciprocal of pK for amino groups of albumin (1.5) [49, 50]; h is the total number of peptide bonds in BSA (0.0088mol/g protein).

Cell culture

Human breast cancer MCF-7 cells were cultured in RPMI 1640 medium containing 10% fetal calf serum and 1% antibiotics (penicillin 10,000 units/mL, streptomycin 10,000μg/mL) at 37 ℃ and 5% CO_2.

Cellular uptake pathway detection

For the uptake inhibition study, MCF-7 cells seeded in 24 well plates were treated with the chemical inhibitors for 0.5h at 37℃. Then the NPs were added to reach a concentration of 37.5μg/mL. After various incubation periods, the effects of the inhibitors on the particle uptake were obtained by both inverted fluorescence microscope observations and quantitative detection. The inhibitors applied in this study included nystatin (25μg/mL)[37] and sucrose (0.45M) [51], which inhibited the caveolae- and clathrin-mediated pathway of endocytosis, respectively.

Cellular uptake kinetic detection

For detection of the intracellular uptake kinetics, the series of albumin NPs diluted by serum-free medium to a concentration of 37.5μg/mL were incubated with MCF-7 cells in 24 well plates at 37℃ and 4℃. After different time intervals (0.5, 1, 2, 4 and 6h), the NP- containing medium was removed, and the cells were washed with cold PBS buffer (pH 8.0). To avoid the interference of rayleigh scattering light in the fluorescence detection, which was caused by the intact cells, the cells had to be splitted, and in consideration that the chemical lysis buffer might interfere the fluorescence detection, the three freeze-thaw method was used for cell splitting[52]. After splitting through three freeze-thaw cycles (-80℃ and 37℃), the cells in each culture well were diluted with PBS buffer (pH 8.0) to a volume of 3 mL and stored at -20℃ until the fluorescence detection in channel D, F and A. After substituting the fluorescence intensities of these channels (F_D, F_F and F_A) into Eq.(3)-Eq.(5), the concentrations of intact and disassociated NPs and the hydrolysis degrees could be obtained by solving the equation group using a sequential scanning method as mentioned in the Section "FRET-based method development".

As internalization uptake was an energy-dependent process, only membrane binding occurred at 4℃, while both binding and uptake took place at 37℃. Therefore, the amount of cell associated nanoparticles at 37℃ was the total amount interacting with cells, and that at 4℃ represented the amount bound to the cell membranes[52-54]. The difference between the amounts at 37℃ and 4℃ represents the intracellular uptake amount.

Intracellular degradation of albumin NPs

To quantify the NPs intracellular degradation, cells seeded in 24-well plates were incubated with the NPs diluted in the serum-free medium (37.5μg/mL) for 2h. After incubation, the medium was replaced by the fresh RPMI 1640 medium, and this time point was set as the starting time (0h) for the degradation detection. At different time points (such as 2, 4, 6 and 8h), the medium was removed, and the cells were washed with cold PBS buffer (pH 8.0). After splitting through three freeze-thaw cycles and dilution with PBS buffer to a volume of 3mL, the samples were stored at -20℃ until fluorescence detection as mentioned above.

Confocal laser microscope observation

The fluorescence signals of the cells in the channel D and channel A could be recorded using the confocal laser scanning microscope (Leica TCS SP5, Leica, Germany) after fixing the cells with 4% paraformaldehyde. The signals in the channel D and A were excited at 488 nm and 543 nm, respectively.

Conclusions

In this study, an albumin NP platform with controllable crosslinking degrees and diameters were prepared using FITC-BSA and $RBITC_{9.5}$-BSA. The cellular uptake and the intracellular fate these albumin NPs were detected quantitatively through a FRET-based method. It was found the albumin NP binding with the cell membrane is rapid and saturated within 1h. The albumin NPs entered MCF-7 cells via the clathrin-mediated endocytosis, which was not affected by the crosslinking degree and diameter of the NPs. However, these NP properties did affect the intracellular uptake of the albumin NPs. The cellular uptake of the albumin NPs increased with the increasing of crosslinking degree (in the range of 42%-92%). The NP number of uptake decreased with the increasing of diameter. However, the cellular uptake increased as diameter increased in terms of NP weight. The albumin NPs cellular degradation behaviour was investigated in the MCF-7 cells. The results indicated that the exocytosis of the NPs was negligible within the 8h. The disassociation rate of the albumin NPs were dependent on the crosslinking degree and diameter of the NPs: with the decreasing of crosslinking degrees and diameters, the disassociation rates increased. The disassociation half-lives of the albumin NPs were found in the range of 35-79h. In MCF-7 cells, the proteins disassociated from the NPs would be hydrolyzed quickly. All these findings provide fundamental information not only for the biological effects and safety of albumin NPs, but also for controlling their properties and intracellular fates which are important for their future drug delivery applications. Furthermore, the FRET-based method developed in this study could provide an applicable tool for the

investigation of NP's intracellular behaviour.

Acknowledgements

This work was supported by the Fundamental Research Funds for the Central Universities (Program No.ZJ11335 and NO. JKPZ2013007), the Natural Science Foundation of Jiangsu Province (Program NO. BK2012355), the National Natural Science Foundation of China (NO. 81402878), and by the College Graduate Research and Innovation Plan of Jiangsu Province (Program No. CXZZ13_0327).

Notes and references

[a] *School of Pharmacy, China Pharmaceutical University, Tongjia Xiang 24, Nanjing, 210009, P.R. China*
[b] *Jiangsu Key Laboratory of New Drug Research and Clinical Pharmacy, School of Pharmacy, Xuzhou Medical College, Tongshan Road 209, Xuzhou, 221004, P.R. China*
[c] *Center for Biomedical Engineering, Department of Medicine, Brigham and Women's Hospital, Harvard Medical School, Boston, MA, 02139, USA.*
[d] *School of Pharmacy, Yancheng Health Vocational & Technical College, Yancheng, 224006, P.R. China*
[e] *University of Waterloo, 200 University Avenue West, Waterloo, ON N2L 3G1, Canada*
[f] *Department of Anesthesia, Brigham and Women's Hospital, Harvard Medical School, Boston, MA, 02139, USA.*
† Electronic Supplementary Information (ESI) available
‡ Both authors contributed equally to this work

1. J. S. Park, M. K. Cho, E. J. Lee, K. Y. Ahn, K. E. Lee, J. H. Jung, Y. Cho, S. S. Han, Y. K. Kim and J. Lee, *Nat Nanotechnol*, 2009, **4**, 259-264.
2. G. Morral-Ruiz, P. Melgar-Lesmes, C. Solans and M. J. Garcia-Celma, *Journal of controlled release : official journal of the Controlled Release Society*, 2013, **171**, 163-171.
3. J. Zhu, Y. Lu, Y. Li, J. Jiang, L. Cheng, Z. Liu, L. Guo, Y. Pan and H. Gu, *Nanoscale*, 2014, **6**, 199-202.
4. R. Xing, G. Liu, J. Zhu, Y. Hou and X. Chen, *Pharmaceutical research*, 2013.
5. Y. Ding, Y. Y. Zhou, H. Chen, D. D. Geng, D. Y. Wu, J. Hong, W. B. Shen, T. J. Hang and C. Zhang, *Biomaterials*, 2013.
6. N. Bertrand, J. Wu, X. Xu, N. Kamaly and O. C. Farokhzad, *Advanced Drug Delivery Reviews*, 2014, **66**, 2-25.
7. N. H. Cho, T. C. Cheong, J. H. Min, J. H. Wu, S. J. Lee, D. Kim, J. S. Yang, S. Kim, Y. K. Kim and S. Y. Seong, *Nat Nanotechnol*, 2011, **6**, 675-682.
8. J. Liu and Y. Lu, *Nat Protoc*, 2006, **1**, 246-252.
9. R. Shrestha, M. Elsabahy, S. Florez-Malaver, S. Samarajeewa and K. L. Wooley, *Biomaterials*, 2012, **33**, 8557-8568.
10. S. Li, J. Zheng, D. Chen, Y. Wu, W. Zhang, F. Zheng, J. Cao, H. Ma and Y. Liu, *Nanoscale*, 2013.
11. J. Wu and C.-C. Chu, *Journal of Materials Chemistry B*, 2013, **1**, 353-360.
12. W. Hai, M. Sujuan, C. Xueqin, Z. Junwei, L. Ming, T. Jianxin, R. Fangfang, D. Yukou, P. Yue and G. Hongwei, *Nanotechnology*, 2014, **25**, 195702.
13. Z. Yu, R. M. Schmaltz, T. C. Bozeman, R. Paul, M. J. Rishel, K. S. Tsosie and S. M. Hecht, *Journal of the American Chemical Society*, 2013, **135**, 2883-2886.
14. J. Wu, D. Yamanouchi, B. Liu and C.-C. Chu, *Journal of Materials Chemistry*, 2012, **22**, 18983-18991.
15. R. P. Singh and P. Ramarao, *Toxicological Sciences*, 2013, **136**, 131-143.
16. H. Gao, W. Shi and L. B. Freund, *Proc Natl Acad Sci U S A*, 2005, **102**, 9469-9474.
17. L. W. Zhang, W. Baumer and N. A. Monteiro-Riviere, *Nanomedicine*, 2011, **6**, 777-791.
18. H. Wartlick, B. Spankuch-Schmitt, K. Strebhardt, J. Kreuter and K. Langer, *Journal of controlled release : official journal of the Controlled Release Society*, 2004, **96**, 483-495.
19. T. Chernenko, C. Matthaus, L. Milane, L. Quintero, M. Amiji and M. Diem, *ACS Nano*, 2009, **3**, 3552-3559.
20. O. Lunov, T. Syrovets, C. Rocker, K. Tron, G. U. Nienhaus, V. Rasche, V. Mailander, K. Landfester and T. Simmet, *Biomaterials*, 2010, **31**, 9015-9022.
21. A. K. Mohammad and J. J. Reineke, *Molecular pharmaceutics*, 2013, **10**, 2183-2189.
22. H. M. Kipen and D. L. Laskin, *American journal of physiology. Lung cellular and molecular physiology*, 2005, **289**, 696-697.
23. P. A. Schulte and F. Salamanca-Buentello, *Environ Health Perspect*, 2007, **115**, 5-12.
24. T. Föster, *Ann. Phys.*, 1948, **2**, 55-75.
25. A. C. Ferreon, J. C. Ferreon, P. E. Wright and A. A. Deniz, *Nature*, 2013, **498**, 390-394.
26. L. Baird, D. Lleres, S. Swift and A. T. Dinkova-Kostova, *Proceedings of the National Academy of Sciences of the United States of America*, 2013, **110**, 15259-15264.
27. H. Kim, H. S. Afsari and W. Cho, *J Lipid Res*, 2013.
28. S. Y. Kim, M. J. Lee, Y. R. Na, S. Y. Kim and E. G. Yang, *J Cell Biochem*, 2013.
29. M. Breunig, U. Lungwitz, R. Liebl and A. Goepferich, *European journal of pharmaceutics and biopharmaceutics : official journal of Arbeitsgemeinschaft fur Pharmazeutische Verfahrenstechnik e.V*, 2006, **63**, 156-165.
30. A. O. Elzoghby, W. M. Samy and N. A. Elgindy, *Journal of controlled release : official journal of the Controlled Release Society*, 2012, **157**, 168-182.
31. J. Han, Q. Wang, Z. Zhang, T. Gong and X. Sun, *Small*, 2013, **doi: 10.1002/smll.201301992.**, .
32. X. Ming, K. Carver and L. Wu, *Biomaterials*, 2013, **34**, 7939-7949.
33. J. Li, Y. Di, C. Jin, D. Fu, F. Yang, Y. Jiang, L. Yao, S. Hao, X. Wang, S. Subedi and Q. Ni, *Nanoscale research letters*, 2013, **8**, 176.
34. M. Satouchi, I. Okamoto, H. Sakai, N. Yamamoto, Y. Ichinose, H. Ohmatsu, N. Nogami, K. Takeda, T. Mitsudomi, K. Kasahara and S. Negoro, *Lung cancer*, 2013, **81**, 97-101.
35. P. Y. Xing, J. L. Li, Y. Wang, X. Z. Hao, B. Wang, L. Yang, Y. K. Shi and X. R. Zhang, *Chinese journal of cancer research = Chung-kuo yen cheng yen chiu*, 2013, **25**, 200-205.
36. Y. Mo, M. E. Barnett, D. Takemoto, H. Davidson and U. B. Kompella, *Mol Vis*, 2007, **13**, 746-757.

37. J. K. Lam, W. Liang, Y. Lan, P. Chaudhuri, M. Y. Chow, K. Witt, L. Kudsiova and A. J. Mason, *Journal of controlled release : official journal of the Controlled Release Society*, 2012, **158**, 293-303.
38. K. Langer, M. G. Anhorn, I. Steinhauser, S. Dreis, D. Celebi, N. Schrickel, S. Faust and V. Vogel, *International journal of pharmaceutics*, 2008, **347**, 109-117.
39. D. L. Lemos, A.L.; Siccardi III, A.J. , *Aquaculture*, 2009, **295**, 89-98.
40. D. S. Kohane, *Biotechnol Bioeng*, 2007, **96**, 203-209.
41. G. J. Doherty and H. T. McMahon, *Annu Rev Biochem*, 2009, **78**, 857-902.
42. A. E. Nel, L. Madler, D. Velegol, T. Xia, E. M. Hoek, P. Somasundaran, F. Klaessig, V. Castranova and M. Thompson, *Nat Mater*, 2009, **8**, 543-557.
43. H. Yuan and S. Zhang, *Applied Physics Letters*, 2010, **96**, 033704.
44. K. Ulbrich, M. Michaelis, F. Rothweiler, T. Knobloch, P. Sithisarn, J. Cinatl and J. Kreuter, *International journal of pharmaceutics*, 2011, **406**, 128-134.
45. L. Jiang, Y. Xu, Q. Liu, Y. Tang, L. Ge, C. Zheng, J. Zhu and J. Liu, *International journal of pharmaceutics*, 2013, **443**, 80-86.
46. D. L. Graham, P. N. Lowe and P. A. Chalk, *Analytical biochemistry*, 2001, **296**, 208-217.
47. G. Hungerford, J. Benesch, J. F. Mano and R. L. Reis, *Photochemical & photobiological sciences : Official journal of the European Photochemistry Association and the European Society for Photobiology*, 2007, **6**, 152-158.
48. E. W. Voss, Jr., C. J. Workman and M. E. Mummert, *BioTechniques*, 1996, **20**, 286-291.
49. M. Karamac and A. Rybarczyk, *Polish Journal of Food and Nutrition Sciences* 2008, **58**, 351-357.
50. D. Shi, Z. He and W. Qi, *Process Biochemistry*, 2005, **40**, 1943-1949.
51. C. N. Antonescu, M. Diaz, G. Femia, J. V. Planas and A. Klip, *Traffic*, 2008, **9**, 1173-1190.
52. Y. Li, J. Wang, Y. Gao, J. Zhu, M. G. Wientjes and J. L. Au, *The AAPS journal*, 2011, **13**, 585-597.
53. N. Düzgüne and N. Shlomo, *Advanced drug delivery reviews*, 1999, **40**, 3-18.
54. K. D. Lee, S. Nir and D. Papahadjopoulos, *Biochemistry*, 1993, **32**, 889-899.